

Unsteady aerodynamics of a pitching NACA 0012 airfoil at low Reynolds number

Dilek Funda Kurtulus 

International Journal of Micro Air

Vehicles

Volume 11: 1–21

© The Author(s) 2019

Article reuse guidelines:

sagepub.com/journals-permissions

DOI: 10.1177/1756829319890609

journals.sagepub.com/home/mav



Abstract

The present paper aims to investigate numerically small amplitude oscillation of NACA 0012 airfoil at $Re = 1000$. The airfoil is sinusoidally pitching around the quarter chord point with 1° pitch amplitude about a mean angle of attack. The computations are performed for mean angles of attack ranging from 0° to 60° and for pitching frequencies of 1 Hz and 4 Hz. The effect of the mean angle of attack and pitching frequency on the instantaneous forces as well as the vortex structure is investigated in comparison with the non-oscillatory conditions. It was shown that airfoil oscillations at the investigated conditions change the amplitude of oscillation of the aerodynamic loads. The instantaneous drag coefficient is always positive for pitching airfoil at 1 Hz. In the meantime, there are time intervals where instantaneous drag coefficient becomes negative for pitching motion at 4 Hz for mean angles of attack from 3° to 36° .

Keywords

Computational Fluid Dynamics, wake pattern, pitching airfoil, micro air vehicle

Date received: 7 June 2019; accepted: 12 October 2019

Introduction

Flapping wing micro air vehicles (MAVs) become much more effective than fixed-wing MAVs as the size of these vehicles decreases.^{1–3} The investigation of the unsteady aerodynamics of pitching airfoils is important for the investigation of animal propulsion, MAV industry, and also for the performance of rotorcrafts⁴ and wind turbine blades.^{5,6} There have been extensive studies in recent years on the flapping wing aerodynamics at low Reynolds (Re) numbers.^{1,7–9}

Pure pitching airfoil is investigated widely at high Re numbers above 50,000.^{10–15} Kim and Chang¹⁶ investigated with smoke-wire flow visualization technique sinusoidally pitching NACA 0012 airfoil at $Re = 23,000$, 33,000, and 48,000 with an oscillating amplitude of 6° and zero mean angle of attack at a reduced frequency of $k = 0.1$. They have also measured unsteady pressure through the pressure correction with pneumatic tubing.

Freytmuth¹⁷ investigated the propulsive wake patterns after NACA 0015 airfoil in pure pitching motions for a reduced frequency of 2.9 and Re number of 12,000. Thrust is generated rather than drag in the

case where the jet-like velocity components are observed at the downstream of the airfoils in plunging or pitching motions.

Koochesfahani¹⁸ experimentally showed the vortical flow patterns in the wake of NACA 0012 airfoil pitching at small amplitudes in a water channel. The experiments are performed at $Re = 12,000$. It is concluded that oscillation frequency, amplitude, and waveform shape affect the structure of the wake. At low frequencies, an undulating vortex pattern is observed. At higher frequencies, an alternating vortex pattern is observed opposite to typical Karman vortex street which corresponds to a jet pattern. This vortex arrangement corresponds to the thrust generating airfoil. He also observed a case with no momentum deficit in the wake (no drag) when the alternating vortices are

Aerospace Engineering Department, METU, Ankara, Turkey

Corresponding author:

Dilek Funda Kurtulus, Aerospace Engineering Department, METU, 06800 Ankara, Turkey.

Email: dfunda@ae.metu.edu.tr



positioned exactly on a straight line. Thrust producing flapping airfoils at different flapping amplitude and frequencies are also presented by Lai and Platzer¹⁹ experimentally.

Bohl and Koochesfahani²⁰ investigated experimentally the flow structure in the wake of a NACA 0012 airfoil pitching around the quarter chord point at a pitch amplitude of 2° about a zero mean angle of attack, and at $Re = 12,600$ using molecular tagging velocimetry technique. The frequency of oscillations is in the range of 1.18 Hz to 3.21 Hz which corresponds to a reduced frequency of 4.1 to 11.5.

Force and particle image velocimetry (PIV) measurements are performed on NACA 0012 airfoil undergoing small amplitude plunge oscillation at $Re = 10,000$ by Clever et al.²¹ They found that local maxima for the lift coefficient occur due to the resonance with the most unstable wake frequency, its subharmonic and first harmonic.

Kurtulus et al.²² investigated experimentally pitching and plunging NACA 0012 airfoil at $Re = 1000$ and compared the results with 2D numerical simulations.

Recently, Tian et al.²³ performed experiments in a closed-circuit low-speed wind tunnel with a symmetric NACA 0012 airfoil model undertaking a sinusoidal pitching motion with 5° pitching amplitude at zero mean angle of attack and at $Re = 3400$. The pitch-pivot-point location was changed from 0.16c to 0.52c with the reduced frequency of the pitching motion ranged from $k = 3.8$ to 13.2. A high-resolution digital PIV system was used to quantify the evolution of the unsteady vortex structures in the wake behind the pitching airfoil.

The effect of the wake patterns for a single flat plate in pitching oscillation motion is studied numerically using a discrete vortex method by Han and Cho²⁴ to investigate possible thrust generation mechanism. They have also investigated two flat plates in pitching oscillations.

Jones et al.²⁵ showed comparison of their panel code results with linear theory of Garrick until reduced frequencies of 20. The efficiency of pitching airfoils converges to 0.5 as a result of linear theory, but panel code reveals lower efficiency values as small as 0.2 for $k = 20$.²⁵

Sarkar²⁶ investigated the effect of non-zero mean angle of attack on the wake of NACA 0012 airfoil at Re number of 10,000 during pure sinusoidally pitch and plunge oscillations using a particle-based Lagrangian viscous solver. The definition of effective angle of attack will lead pure plunge case to an equivalent pure-pitch case, but the selection of the mean angle of attack is also an important parameter for the comparison. The wake deflection depends on the total

angle of attack and not only the amplitude of the pitching oscillation.

Sarkar and Venkatraman²⁷ studied dynamic stall of NACA 0012 airfoil with reduced frequencies ranging from 0.5 to 3.0 oscillating at an amplitude of 10° around a mean angle of attack of 15° and oscillating at an amplitude of 20° and mean angle of attack of 25° . The simulations are performed at $Re = 10,000$, and it is noted that the pitching angle of an oscillating airfoil in the post stall regime impacts its dynamic behavior significantly.

Medjroubi et al.²⁸ investigated NACA 0012 airfoil oscillating in heave (plunge) motion at mean incidences of 12° to 20° at $800 \leq Re \leq 10,000$ solving Navier–Stokes equations using a Spectral/hp Element method for spatial discretization. They concluded that increasing Re number while keeping the same frequency and amplitude of oscillations has no major effects neither on flow structure nor on the aerodynamic loads; however, the mean incidence angle influences dominantly the flowfield. They stated that setting the airfoil in motion has the same effect as for increasing the mean angle of attack for steady airfoils.

Pitching and plunging NACA 0012 airfoil at Re number of 1000 was presented by Khalid et al.²⁹ They have proposed a novel criterion based on the Strouhal number which provides equivalence of pitching and plunging motions taking into account the length scale traversed by the corresponding trailing edges.

Although there are lots of studies about the vortex patterns at the wake of the airfoils around pitching/flapping airfoils at low Re numbers, the characteristics of the wake patterns are not investigated at small pitch amplitudes around different mean angles of attack. In addition, there are very few data available in literature about pure pitching oscillations at low Re numbers of order 1000. Kurtulus^{30,31} previously investigated the flow past NACA 0012 and NACA 0002 airfoils at $Re = 1000$ for steady uniform flow at different incidence angles. She has classified the wake structures into five different modes (Kurtulus modes³²) according to their pattern obtained from instantaneous and mean vorticity fields by also taking into account the amplitude spectrum of the lift coefficient, the instantaneous and mean aerodynamic force coefficients, velocity fields, and the longitudinal and lateral vortex spacings. Rossi et al.³² show that the classification of the wake structures is similarly visualized for Re number ranging from 100 to 3000.

Kurtulus³³ also showed that the mean lift coefficient increases slightly for 1 Hz pitching motion for the mean angles of attack lower than 15° ; however, it decreases for 4 Hz pitching motion compared to non-oscillatory airfoil. The lift curve slope at zero angle of attack has

been found to be approximately π for NACA 0012 airfoil at $Re = 1000$ for non-oscillatory condition, and it is found that pitching the NACA 0012 airfoil around zero mean angle of attack at 1 Hz slightly increases the lift curve slope; however, pitching the same airfoil at 4 Hz results a decrease in the lift curve slope.

In the current study, the unsteady flow structures around a pitching NACA 0012 with an amplitude of 1° about a mean angle of attack at a low Re number of 1000 are investigated. The airfoil oscillates sinusoidally in pitch about its quarter chord axis with a frequency of 1 Hz and 4 Hz about the mean angles of attack which varies in the range of 0° – 60° . These frequencies are selected based on the previous findings from the amplitude spectrum of the lift coefficient for the non-oscillatory NACA 0012 airfoil at $Re = 1000$ where a maximum vortex shedding frequency of $f = 1.3$ Hz was obtained at 9° angle of attack.³⁰

The main motivation of the current paper was to investigate the effect of the very small disturbances like 1° oscillations to vortex patterns in addition to aerodynamic forces in order to better understand in general the flapping airfoil vortex formation and compare the results with the previous steady airfoil simulations. In order to have an idea about the frequency effect, the results are presented at two different frequencies.

The numerical simulations are performed using a finite-volume-based package program ANSYS Fluent. The flow structure analysis includes the vortex formation, wake shedding frequency, and their effects on aerodynamic coefficients. The vortex patterns at two different reduced frequencies for different mean angle of attacks are compared. Their effects on the instantaneous aerodynamic loads are discussed.

Numerical method

Governing equations and geometry

The governing equations are Navier–Stokes equations for incompressible, laminar, and two-dimensional flow

$$\bar{\nabla} \cdot \bar{V} = 0 \quad (1)$$

$$\frac{\partial \bar{V}}{\partial t} + \left(\bar{V} \cdot \bar{\nabla} \right) \bar{V} = -\frac{1}{\rho} \bar{\nabla} p + \nu \nabla^2 \bar{V} \quad (2)$$

ANSYS Fluent implements the finite-volume method to solve conservation equations. The pressure–velocity coupling is done by means of the SIMPLE-type fully implicit algorithm. Pressure–velocity coupling is used with a predictor–corrector pressure scheme. Transient solution has been approximated

using second order implicit method. The solution is second-order accurate in space and time. The velocity inlet boundary condition is used at the semi-circular region of the outer domain, and pressure outlet is used at the other side of the outer region. The far field boundary is located at $15c$ away from the airfoil.

The instantaneous angle of attack, α , defined to be positive in the clockwise direction was varied sinusoidally (equation (3)) with an amplitude of 1° ($A = 1^\circ$), and with frequencies of $f = 1$ Hz and $f = 4$ Hz around a mean incidence angle (α_0). The effect of mean incidence angle is investigated from $\alpha_0 = 0^\circ$ to $\alpha_0 = 60^\circ$ with an increment step of 1° for $\alpha_0 < 40^\circ$ and 10° for $40^\circ \leq \alpha_0 \leq 60^\circ$

$$\alpha = \alpha_0 + A \sin(2\pi ft) \quad (3)$$

The instantaneous angular velocity Ω is given by equation (4)

$$\Omega = A(2\pi f) \cos(2\pi ft) \quad (4)$$

The pivot point was at the quarter chord location (0.25c) from the leading edge of the airfoil. Reduced frequency is $k = 2\pi fc / U_\infty$ where $U_\infty = 0.146$ m/s, $c = 0.1$ m, and pitching frequency is taken to be $f = 1$ Hz and $f = 4$ Hz which results the reduced frequencies as 4.3 and 17.2, respectively. Re number is 1000.

Grid and time refinement studies have been carried out for steady NACA 0012 airfoil in a previous study by Kurtulus.³⁰ The steady aerodynamic force coefficients are also compared in this previous study for NACA 0012 airfoil with different data available in literature,^{34–38} and the results are found to be very similar. In addition, the mean lift and drag coefficients for a thinner airfoil (NACA 0002) were previously compared with the results of Kunz and Kroo³⁹ which were available for angle of attack values of 0° to 8° at steady conditions. The results are similarly found to be very close to each other.³¹ The same number of grid and time increments is also used in the current study. Three hundred nodes are used around the airfoil for the medium mesh selected after the grid refinement study compared to 150 nodes at coarse grid and 500 nodes at fine grid. The first cell spacing of the boundary layer for medium mesh has value of $0.0015c$. Total number of elements is order of 200,000. The mesh around the airfoil is composed of two parts, namely inner region and outer region. The inner region above the boundary layer is constructed with a semi-circle having radius of $1.5c$ centered at the airfoil $c/4$ location at the upstream and a rectangular region with width of $1.5c$ at the downstream of the airfoil. The inner region mesh is unstructured triangular grid. The outer domain is of C-type structured mesh. The far field boundary is

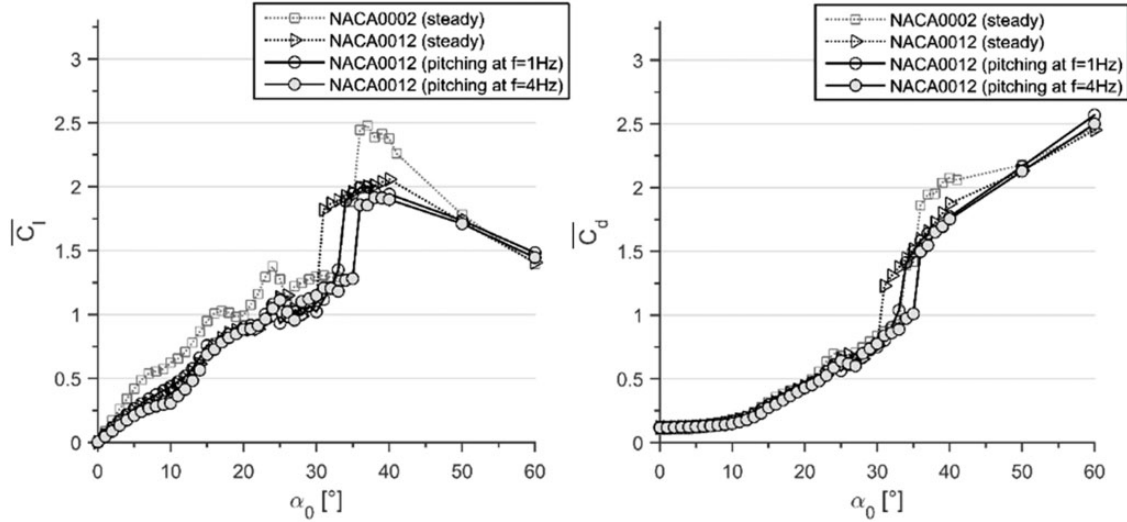


Figure 1. Mean aerodynamic lift and drag coefficients for NACA 0012 pitching at $f = 1$ Hz and $f = 4$ Hz in comparison with the non-oscillatory NACA 0012 and NACA 0002 airfoils at $Re = 1000$.

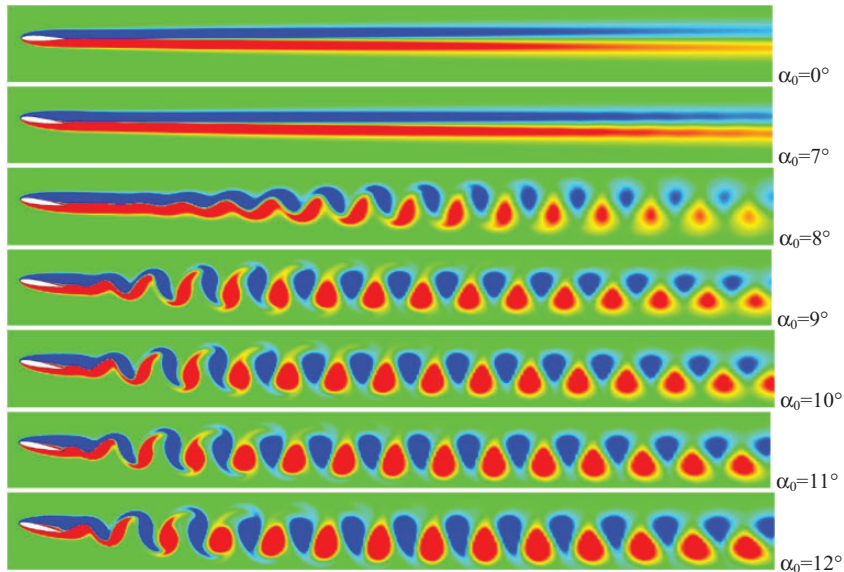


Figure 2. Instantaneous vorticity distribution for non-oscillating NACA 0012 ($t = 100$ s) at $Re = 1000$.

located at $15c$ upstream and $19c$ downstream from the leading edge of the airfoil. With the preprocessor program, the airfoil is rotated for the given angle of attack in the inner region by keeping the outer domain and wake region fixed with the same structured grid. The time refinement study carried out with time increments of $\Delta t = 0.0005$ s, $\Delta t = 0.005$ s, and $\Delta t = 0.001$ s reveals that $\Delta t = 0.005$ s in comparison with $\Delta t = 0.0005$ s give almost same results; therefore, the current study is performed with time increment of $\Delta t = 0.005$ s. This time increment was also selected in the previous studies for steady conditions.^{30,31} For pitching conditions, the computational time interval is 36 s, and the mean

vorticity contours are obtained in the interval of $t \in [16 \text{ s } 36 \text{ s}]$. C_l and C_d denote the instantaneous lift and drag coefficients for the airfoil, respectively. It should be noted that for the steady solutions, the results were simulated until $t = 100$ s, and the mean contours and values were obtained by averaging in the interval of $50 \text{ s} \leq t \leq 100 \text{ s}$.

Results

Unsteady numerical simulation past a sinusoidally pitching airfoil with 1° pitching amplitude at two different pitching frequencies has been performed and

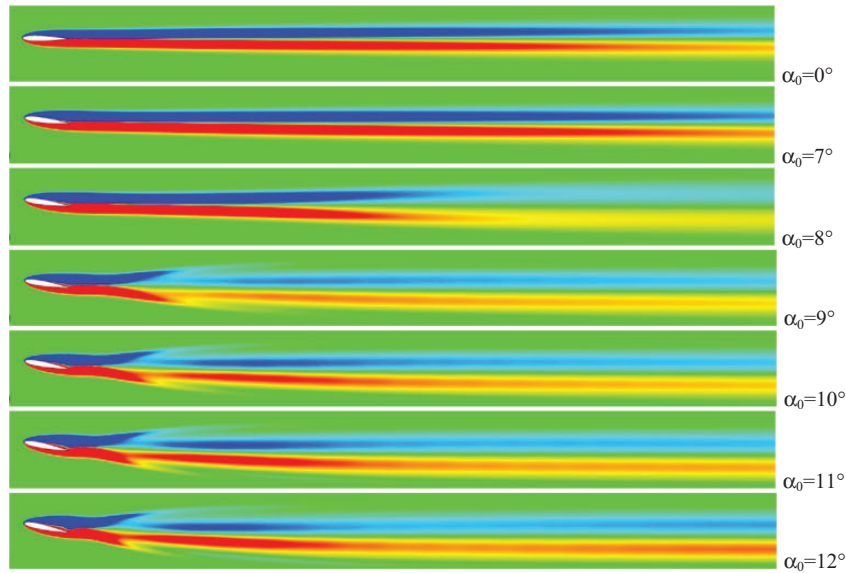


Figure 3. Mean vorticity distribution for non-oscillating NACA 0012 at $Re = 1000$.

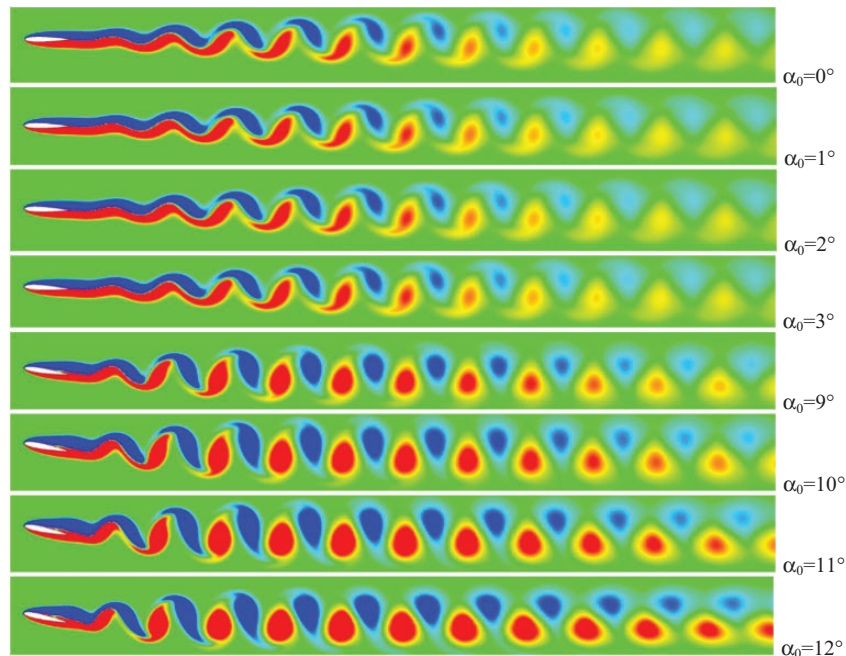


Figure 4. Instantaneous vorticity distribution for NACA 0012 airfoil oscillating at $f = 1$ Hz ($t = 36$ s).

compared with the non-oscillatory results. The airfoil is pitching about its quarter chord point.

Mean aerodynamic coefficients

The effect of small amplitude pitching oscillation on NACA 0012 airfoil is already investigated on mean aerodynamic coefficients,³³ and the results are

compared with the non-oscillatory simulations of previous studies.^{30,31} The comparison of mean lift coefficient, mean drag coefficient, and mean lift to drag coefficient ratios for pitching NACA 0012 airfoil at $f = 1$ Hz and $f = 4$ Hz are performed in comparison with the non-oscillatory solutions for NACA 0012 and a thinner airfoil NACA 0002³¹ at $Re = 1000$ as shown in Figure 1. The detailed discussion about the

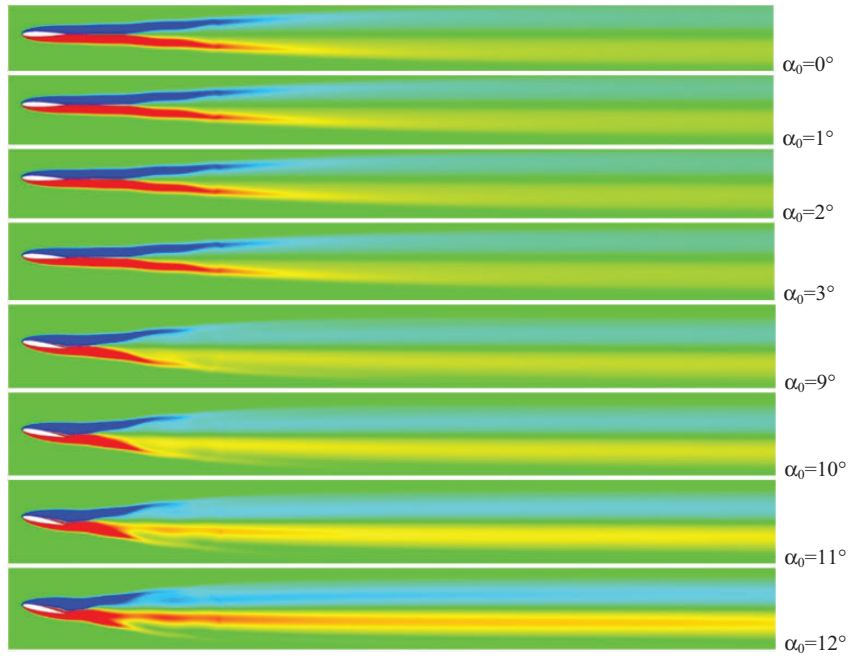


Figure 5. Mean vorticity distribution for NACA 0012 airfoil oscillating at $f = 1$ Hz.

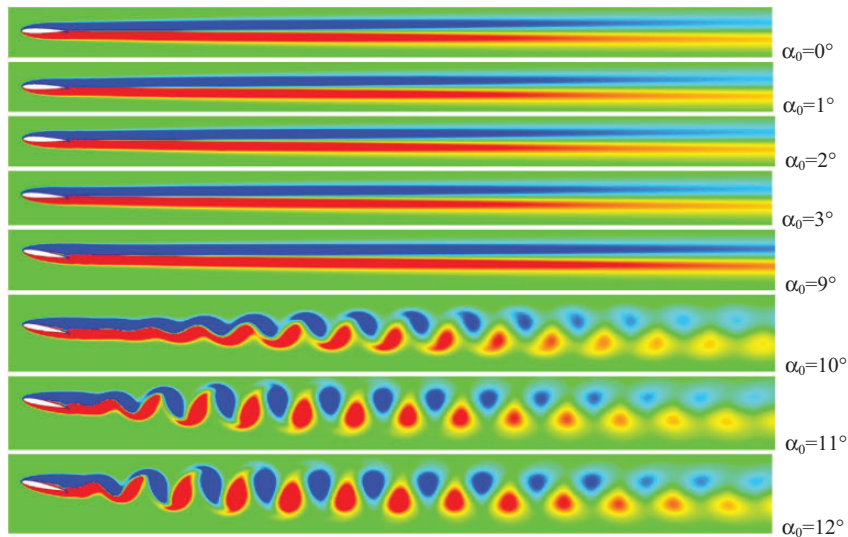


Figure 6. Instantaneous vorticity distribution for NACA 0012 airfoil oscillating at $f = 4$ Hz ($t = 36$ s).

mean lift, drag, and lift-to-drag ratios are given in Kurtulus.³³

It is observed that the mean values are slightly affected by the small amplitude pitching motion of the airfoil; however, there is an important change in the instantaneous aerodynamic forces and specifically in the oscillation amplitudes of these coefficients. The pitching motion also alters the wake

shedding behind the airfoil compared to non-oscillatory cases.

Comparison of instantaneous and mean wake patterns

The instantaneous and mean vorticity contours are presented for steady airfoil (Figures 2 and 3), for $f = 1$ Hz

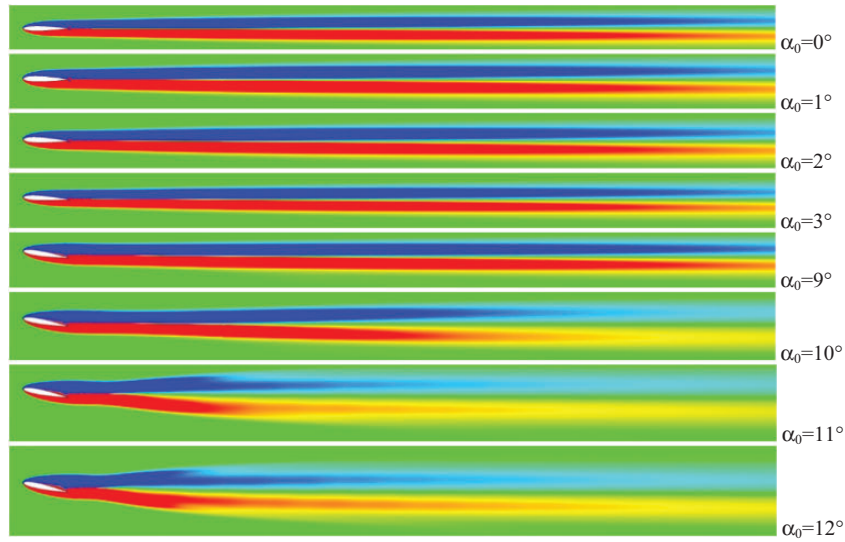


Figure 7. Mean vorticity distribution for NACA 0012 airfoil oscillating at $f = 4$ Hz.

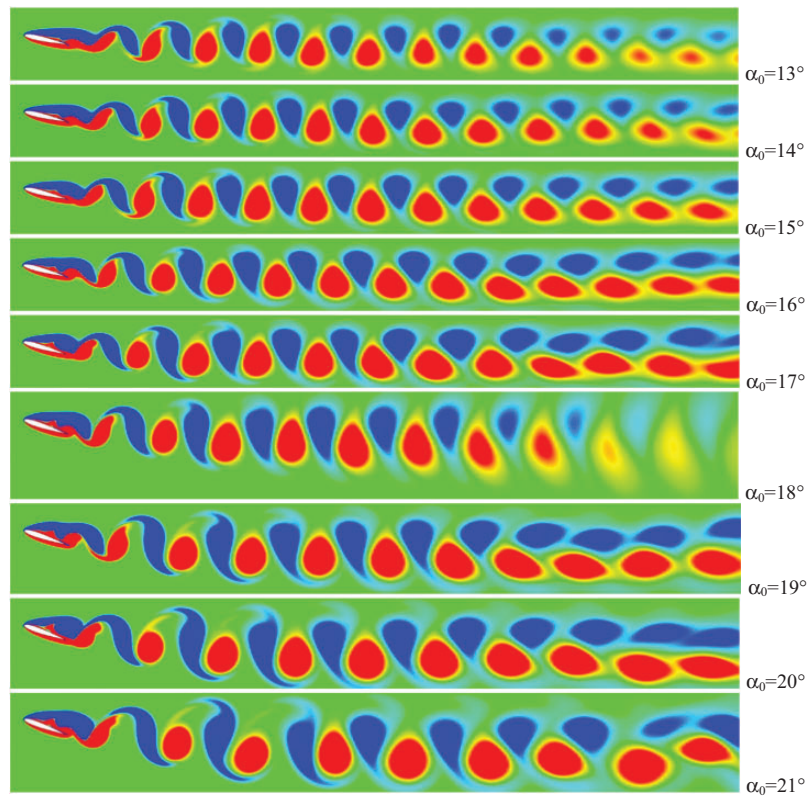


Figure 8. Instantaneous vorticity distribution for NACA 0012 airfoil oscillating at $f = 4$ Hz ($t = 36$ s).

oscillation (Figures 4 and 5) and for $f = 4$ Hz (Figures 6 and 7) for same angles of attack below 12° to present the oscillation frequency influence to the wake shedding of the NACA 0012 airfoil at $Re = 1000$.

It was previously found that instantaneous and mean vortex shedding are similar and almost straight for the angles of attack less than or equal to $\alpha_0 = 7^\circ$ at steady conditions, and a periodic vortex shedding is

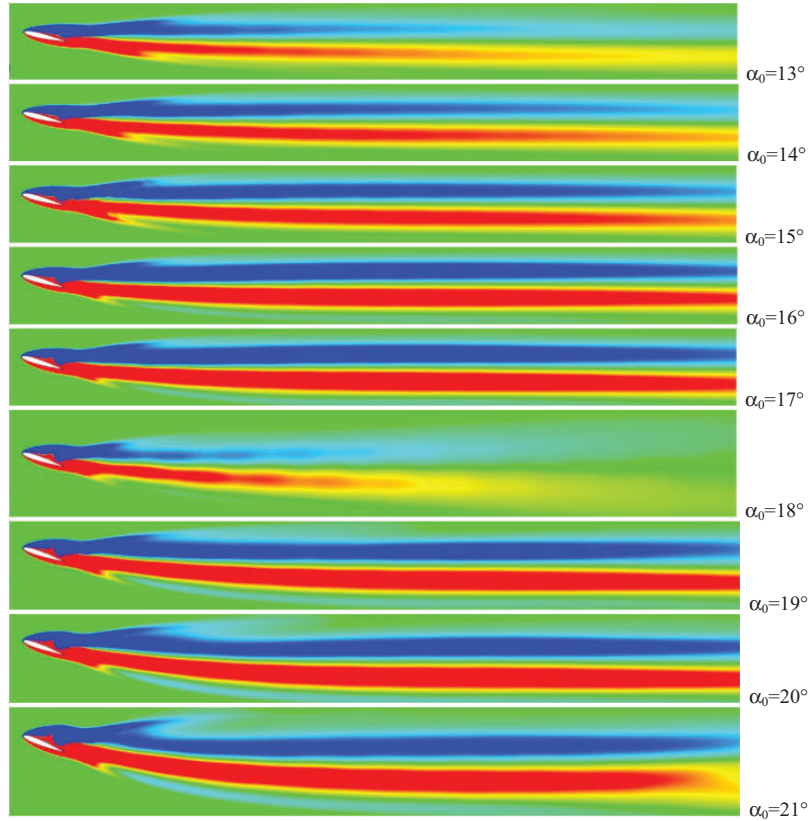


Figure 9. Mean vorticity distribution for NACA 0012 airfoil oscillating at $f = 4$ Hz.

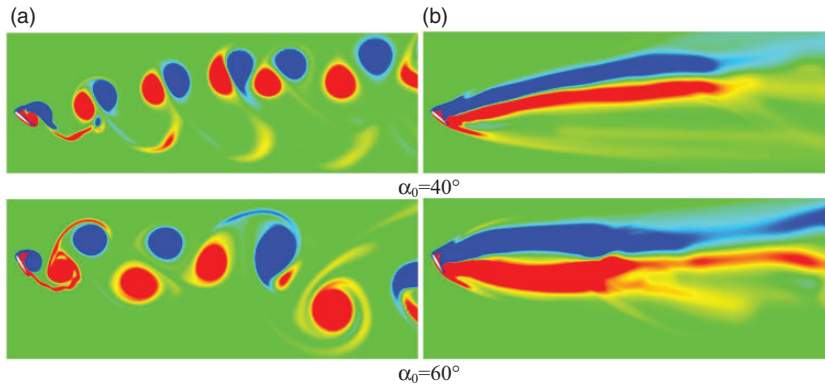


Figure 10. Vorticity distribution for NACA 0012 airfoil oscillating at $f = 4$ Hz. (a) Instantaneous ($t = 36$ s). (b) Mean.

observed above $\alpha_0 = 8^\circ$.³⁰ For $f = 4$ Hz pitching oscillations, the periodic vortex shedding is observed at a higher mean angle of attack of 10° (Figures 6 and 7). In contrast, the periodic vortex shedding can be visualized for all angles of attack of the NACA 0012 airfoil oscillating at $f = 1$ Hz frequency (Figures 2 and 3).

The instantaneous and mean vorticity distributions for $f = 4$ Hz are analyzed in Figures 8 and 9 for α_0 ranging from 13° to 21° , respectively. The wake pattern of the airfoil is observed to alter at the downstream of the airfoil above $\alpha_0 = 13^\circ$. The amplitude spectrum of C_1 at $f = 4$ Hz reveals also an abrupt increase in the frequency spectrum at $\alpha_0 = 13^\circ$ compared to $\alpha_0 = 12^\circ$

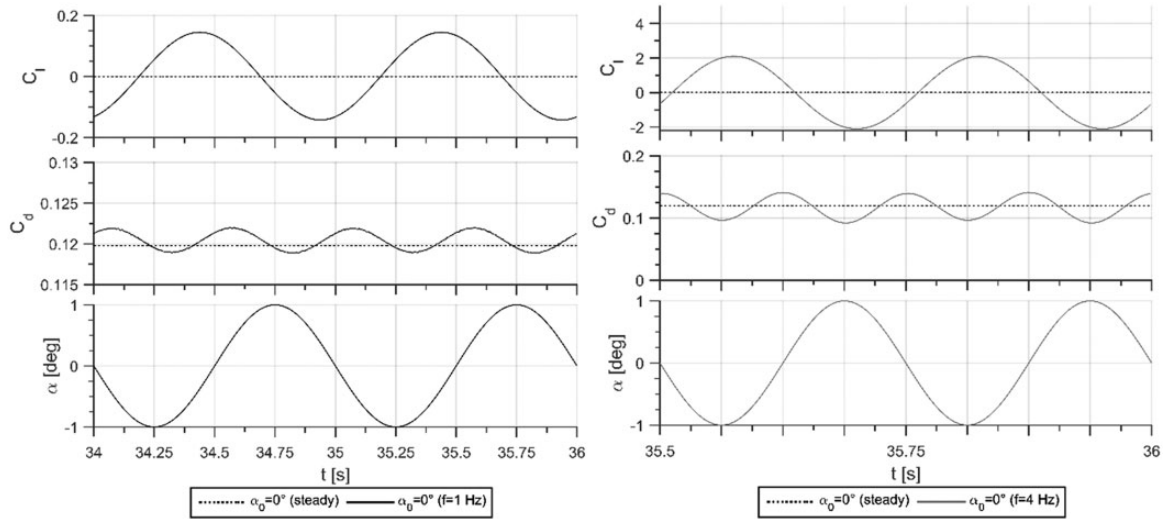


Figure 11. Instantaneous lift and drag coefficients for $f = 1$ Hz and $f = 4$ Hz oscillations at $\alpha_0 = 0^\circ$.

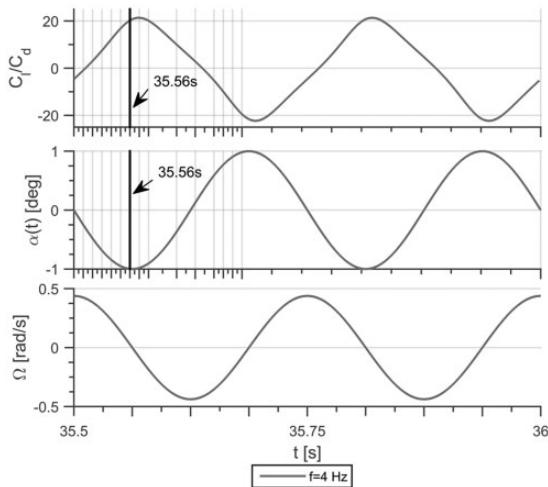


Figure 12. C_l/C_d ratio, instantaneous angle of attack, and angular velocity versus time for $f = 4$ Hz oscillations at $\alpha_0 = 0^\circ$.

as shown in Figure 20. The wake height also increases with the mean angle of attack, and the alternating vortices start to merge from the far downstream to the vortices at their upstream as the mean angle of attack increases until $\alpha_0 = 17^\circ$. At mean angle of attack of 18° , a transition of the wake distribution is observed, and at $\alpha_0 = 21^\circ$ the vortices start to lose their instantaneous alternating pattern at the far downstream (Figure 8). The mean vorticity contours show the increase of the

wake height with the mean angle of attack which is also a reason for the increase of drag coefficient (Figure 9).

The instantaneous and mean vorticity contours at higher mean angles of attack (40° and 60°) are presented in Figure 10(a) and (b), respectively. At high angles of attack it is observed that the shedding frequency decreases, and more K-H vortices are amalgamated to form one Karman vortex.^{30,40,41}

Comparison of instantaneous aerodynamic coefficients

Instantaneous aerodynamic coefficients for different angles of attack are presented below for pitching airfoil at $f = 1$ Hz and $f = 4$ Hz in comparison with the steady airfoil. It is observed that the instantaneous drag coefficient is always positive for $f = 1$ Hz simulations (Figures 11 and 15 to 18). However, unsteady drag coefficient is always positive for pitching airfoil around 0° , 1° , and 2° mean angle of attacks for $f = 4$ Hz. Between $3^\circ \leq \alpha_0 \leq 36^\circ$, there are local time intervals where drag coefficient becomes negative (thrust) for $f = 4$ Hz pitching motion. Transition mean angles of attack are 37° and 38° , and above these mean angle of attacks, the instantaneous drag coefficient is all through positive.

The aerodynamic coefficients of the airfoil pitching around $\alpha_0 = 0^\circ$ are periodic, and they have sinusoidal patterns both at $f = 1$ Hz and $f = 4$ Hz (Figure 11). It is noted that these two cases are the only cases among the

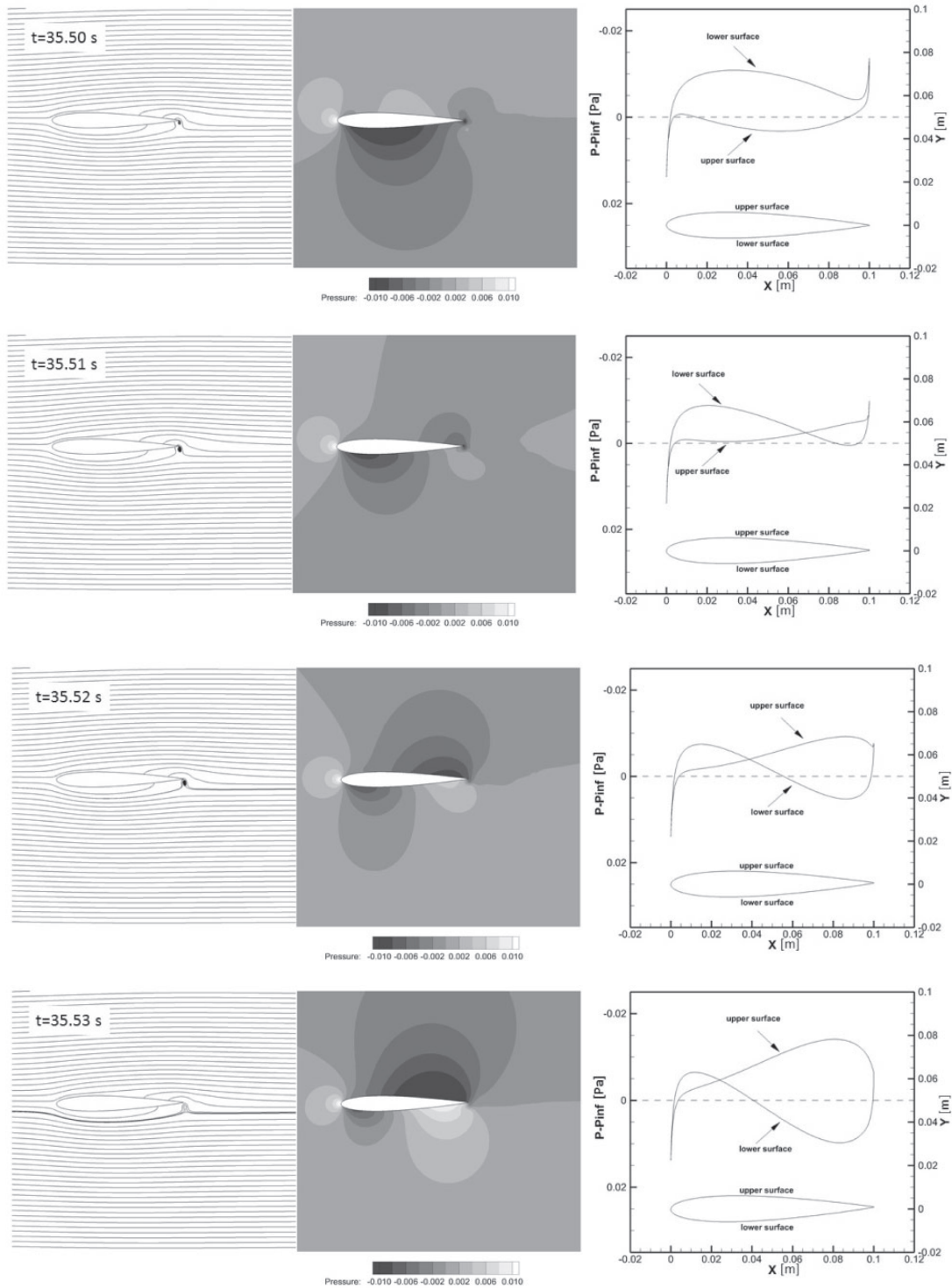


Figure 13. Instantaneous streamlines, gauge pressure contours, and wall gauge pressure at $f = 4$ Hz oscillation and $\alpha_0 = 0^\circ$ during pitch down motion.

$t = 35.50$ s; $\alpha = 0^\circ$; $\Omega = 0.4386$ rad/s; $C_l = -0.4776$; $C_d = 0.1396$; $C_l/C_d = -3.4202$.

$t = 35.51$ s; $\alpha = -0.2487^\circ$; $\Omega = 0.4249$ rad/s; $C_l = -0.2151$; $C_d = 0.1386$; $C_l/C_d = -1.5526$.

$t = 35.52$ s; $\alpha = -0.4818^\circ$; $\Omega = 0.3844$ rad/s; $C_l = 0.3153$; $C_d = 0.1327$; $C_l/C_d = 2.3764$.

$t = 35.53$ s; $\alpha = -0.6845^\circ$; $\Omega = 0.3198$ rad/s; $C_l = 0.8253$; $C_d = 0.1228$; $C_l/C_d = 6.7203$.

$t = 35.54$ s; $\alpha = -0.8443^\circ$; $\Omega = 0.2350$ rad/s; $C_l = 1.2818$; $C_d = 0.119$; $C_l/C_d = 11.455$.

$t = 35.55$ s; $\alpha = -0.9511^\circ$; $\Omega = 0.1356$ rad/s; $C_l = 1.6570$; $C_d = 0.1025$; $C_l/C_d = 16.1666$.

$t = 35.56$ s; $\alpha = -0.9980^\circ$; $\Omega = 0.0275$ rad/s; $C_l = 1.9281$; $C_d = 0.097$; $C_l/C_d = 19.8711$.

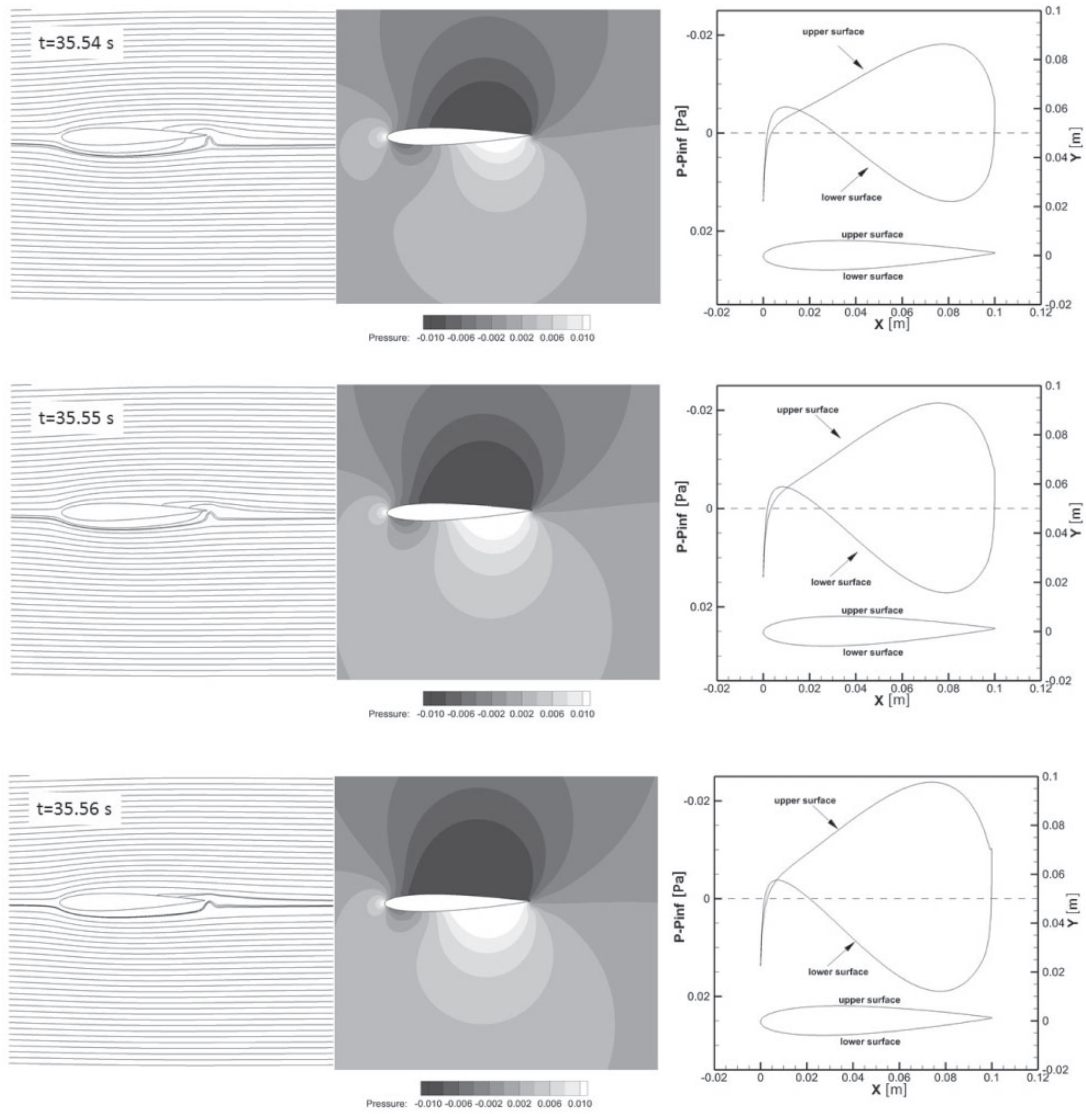


Figure 13. Continued.

simulated results where a period doubling is observed in a sinusoidal form for the drag coefficient.

There is a suction region at the lower side of the airfoil at the beginning of the period where the airfoil pitch down at $f = 4$ Hz. Figure 12 shows that the lift-to-drag ratio increases during the pitch down motion of the airfoil in the interval of $t \in [35.5 \text{ s } 35.56 \text{ s}]$. In this interval, the lift-to-drag ratio increase resulted due to a simultaneous increase in the lift coefficient and decrease in the drag coefficient. Figures 13 and 14 show instantaneous streamlines, gauge pressure contours, and wall gauge pressure on the airfoil at $f = 4$ Hz oscillation and $\alpha_0 = 0^\circ$ during pitch down and pitch up motions, respectively.

When the mean angle of attack increases to 1° , a deviation from sinusoidal behavior is observed for the drag coefficient (Figure 15). For the lift coefficient of the airfoil oscillating at $f = 4$ Hz, the sinusoidal behavior is observed for all cases investigated. However, the amplitude of the sinusoidal function stays constant until $\alpha_0 = 11^\circ$ in the quasi-steady region for $f = 4$ Hz (Figure 16). For the airfoil oscillating at $f = 1$ Hz, the lift coefficient deviates from the sinusoidal behavior above $\alpha_0 = 11^\circ$ as can be observed clearly from Figures 16 and 17.

The minimum C_d value decreases specifically for $f = 4$ Hz oscillation, and negative C_d values are observed above mean angles of attack of 3° (Figure 15) until a mean angle of attack of 37° .

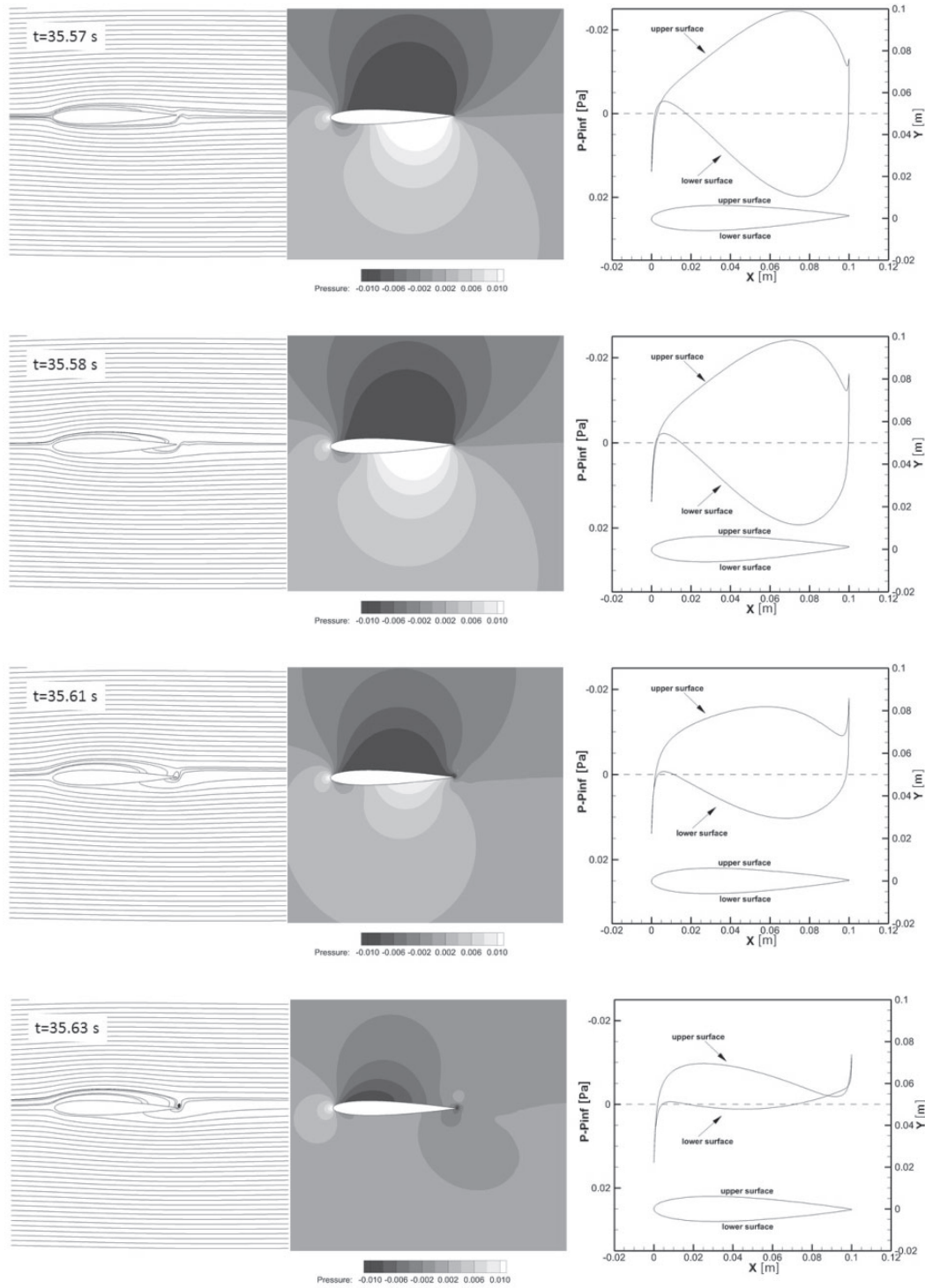


Figure 14. Instantaneous streamlines, gauge pressure contours, and wall gauge pressure at $f = 4$ Hz oscillation and $\alpha_0 = 0^\circ$ during pitch up motion.

$t = 35.57$ s; $\alpha = -0.9823^\circ$; $\Omega = -0.0822$ rad/s; $C_l = 2.0792$; $C_d = 0.0972$; $C_l/C_d = 21.3996$.

$t = 35.58$ s; $\alpha = -0.9048^\circ$; $\Omega = -0.1868$ rad/s; $C_l = 2.1019$; $C_d = 0.1026$; $C_l/C_d = 20.4792$.

$t = 35.61$ s; $\alpha = -0.3681^\circ$; $\Omega = -0.4078$ rad/s; $C_l = 1.4151$; $C_d = 0.1333$; $C_l/C_d = 10.6141$.

$t = 35.63$ s; $\alpha = 0.1253^\circ$; $\Omega = -0.4352$ rad/s; $C_l = 0.4827$; $C_d = 0.1409$; $C_l/C_d = 3.4253$.

$t = 35.65$ s; $\alpha = 0.5878^\circ$; $\Omega = -0.3549$ rad/s; $C_l = -0.5696$; $C_d = 0.1270$; $C_l/C_d = -4.4859$.

$t = 35.66$ s; $\alpha = 0.7705^\circ$; $\Omega = -0.2796$ rad/s; $C_l = -1.0568$; $C_d = 0.1152$; $C_l/C_d = -9.1777$.

$t = 35.67$ s; $\alpha = 0.9048^\circ$; $\Omega = 0.1868$ rad/s; $C_l = -1.4757$; $C_d = 0.1037$; $C_l/C_d = -14.2332$.

$t = 35.68$ s; $\alpha = 0.9823^\circ$; $\Omega = -0.0822$ rad/s; $C_l = -1.8010$; $C_d = 0.0953$; $C_l/C_d = -18.9006$.

The bold values are angle of attack, angular velocity, lift coefficient, drag coefficient and C_l/C_d ratio at the given instantaneous time. For $t = 35.57$ s then at time $t = 35.58$ s etc.

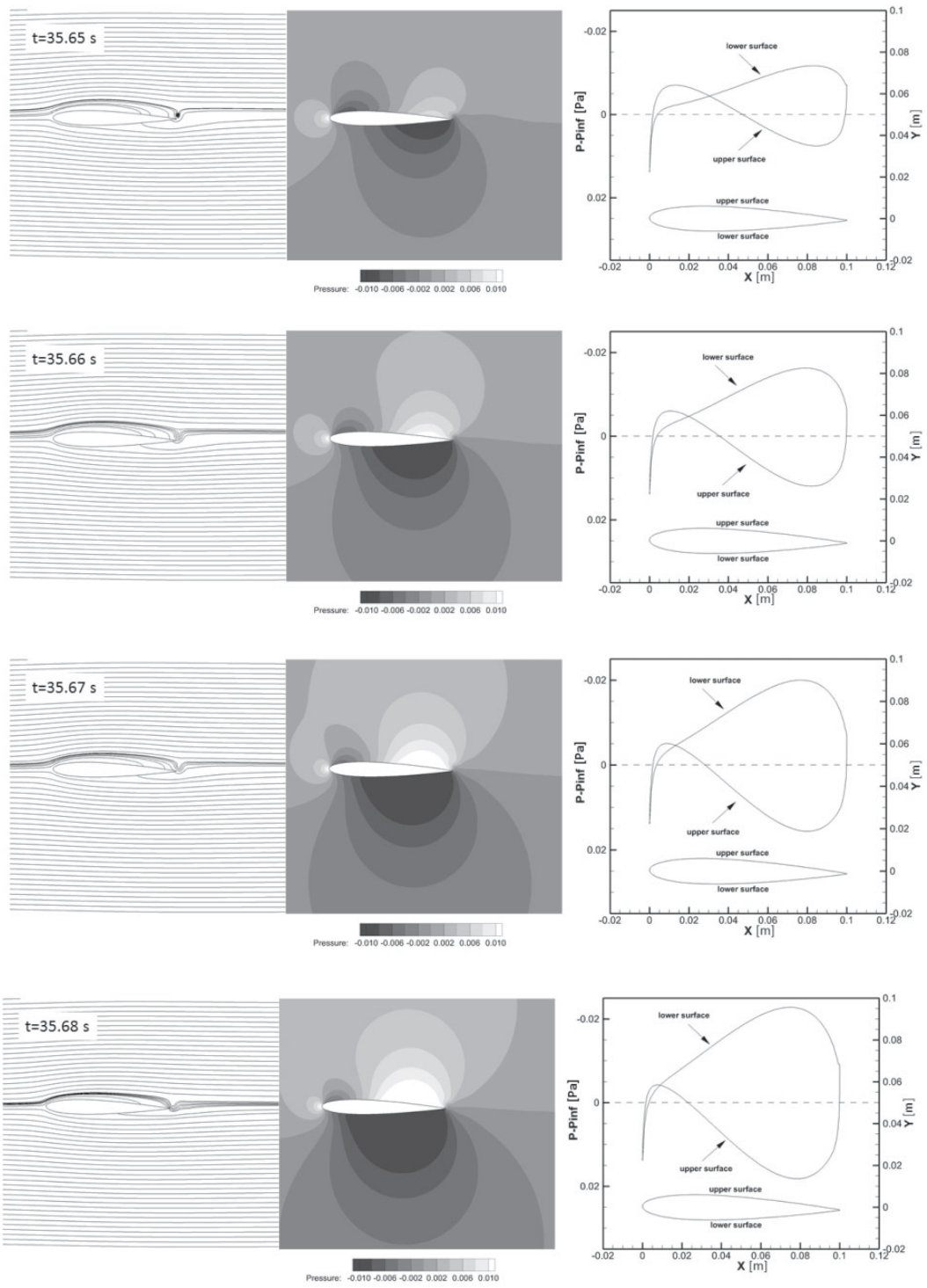


Figure 14. Continued.

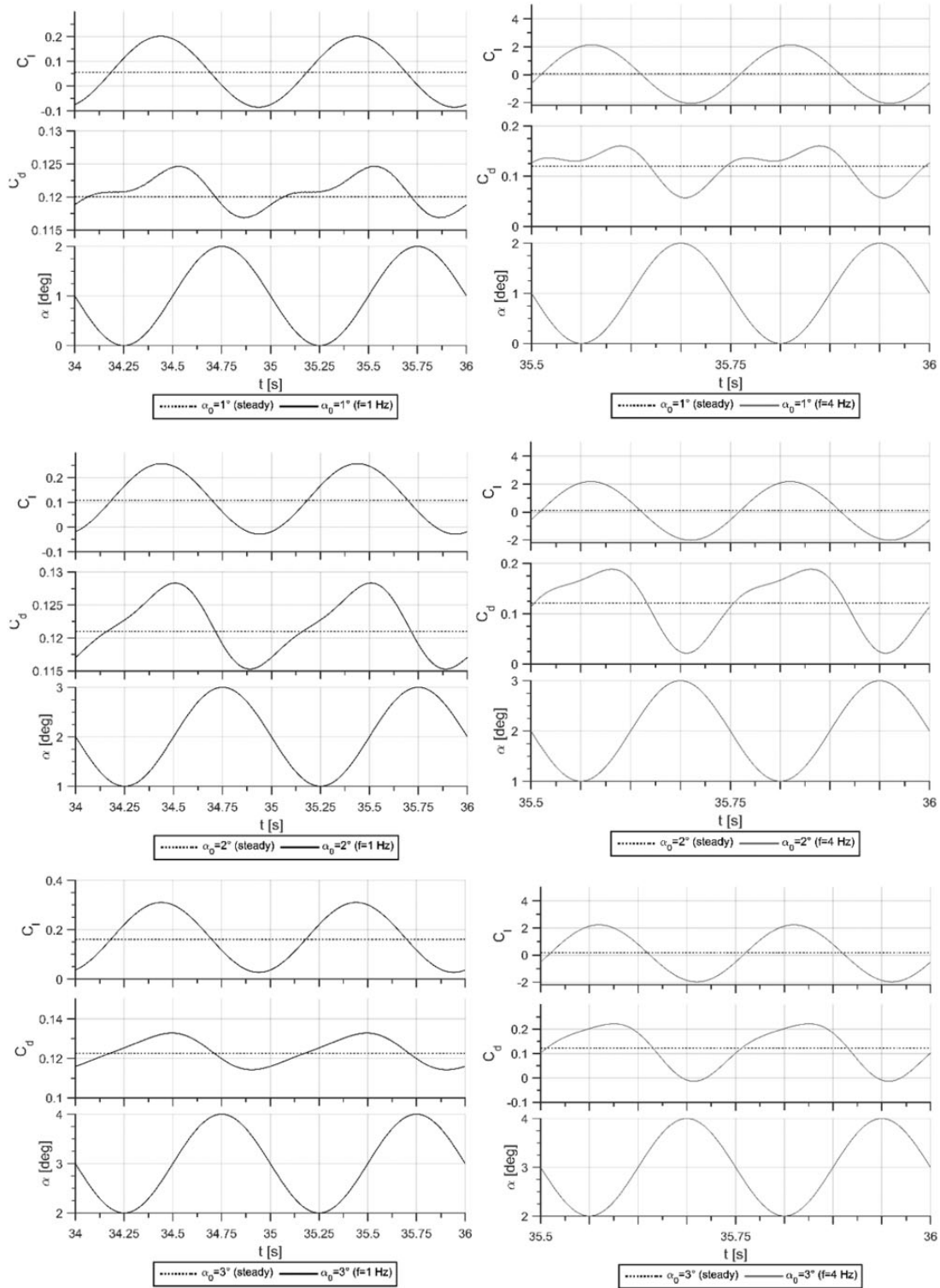


Figure 15. Instantaneous lift and drag coefficients for $f = 1$ Hz and $f = 4$ Hz oscillations at $\alpha_0 = 1^\circ$, 2° , and 3° .

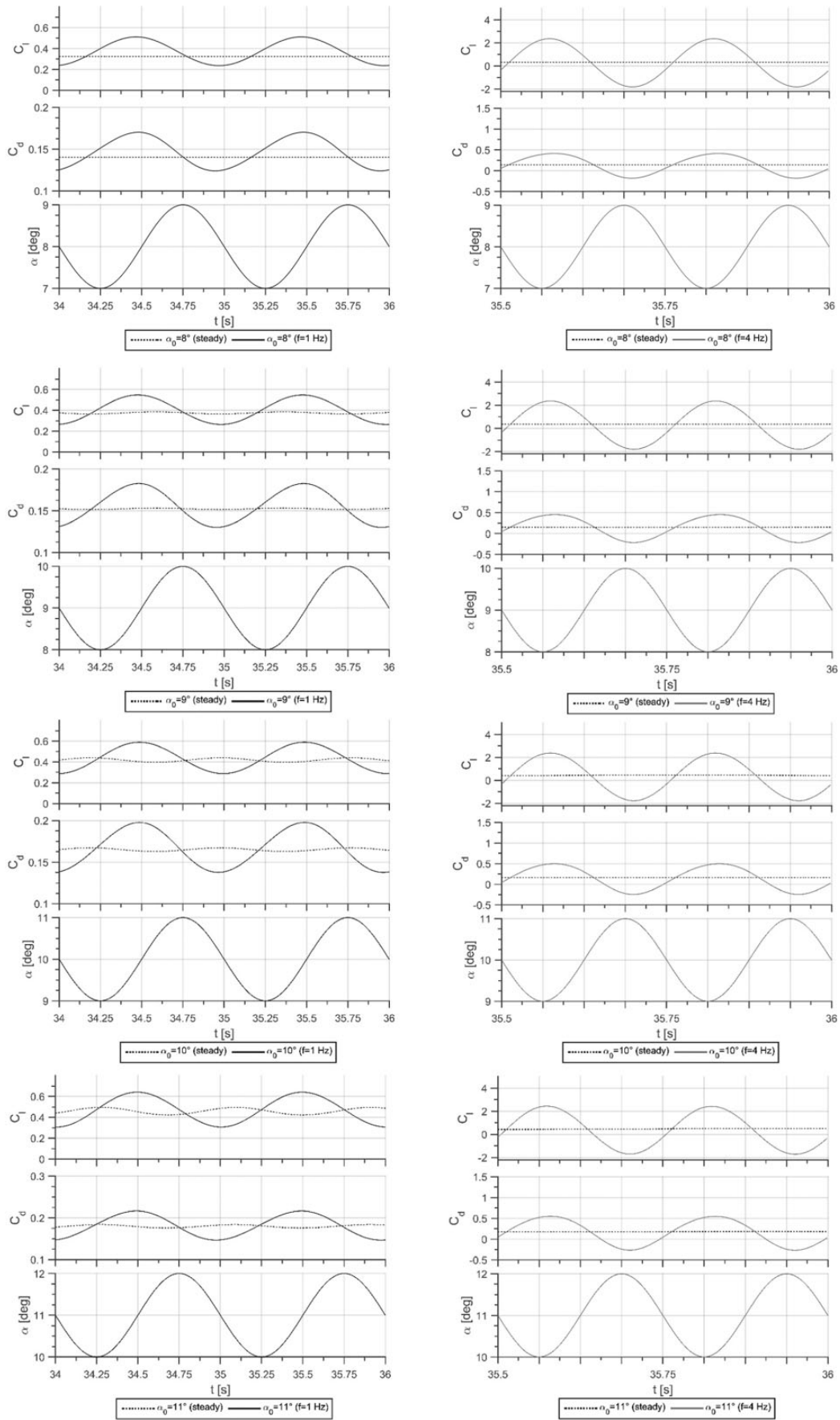


Figure 16. Instantaneous lift and drag coefficients for $f = 1$ Hz and $f = 4$ Hz oscillations at $\alpha_0 = 8^\circ, 9^\circ, 10^\circ, \text{ and } 11^\circ$.

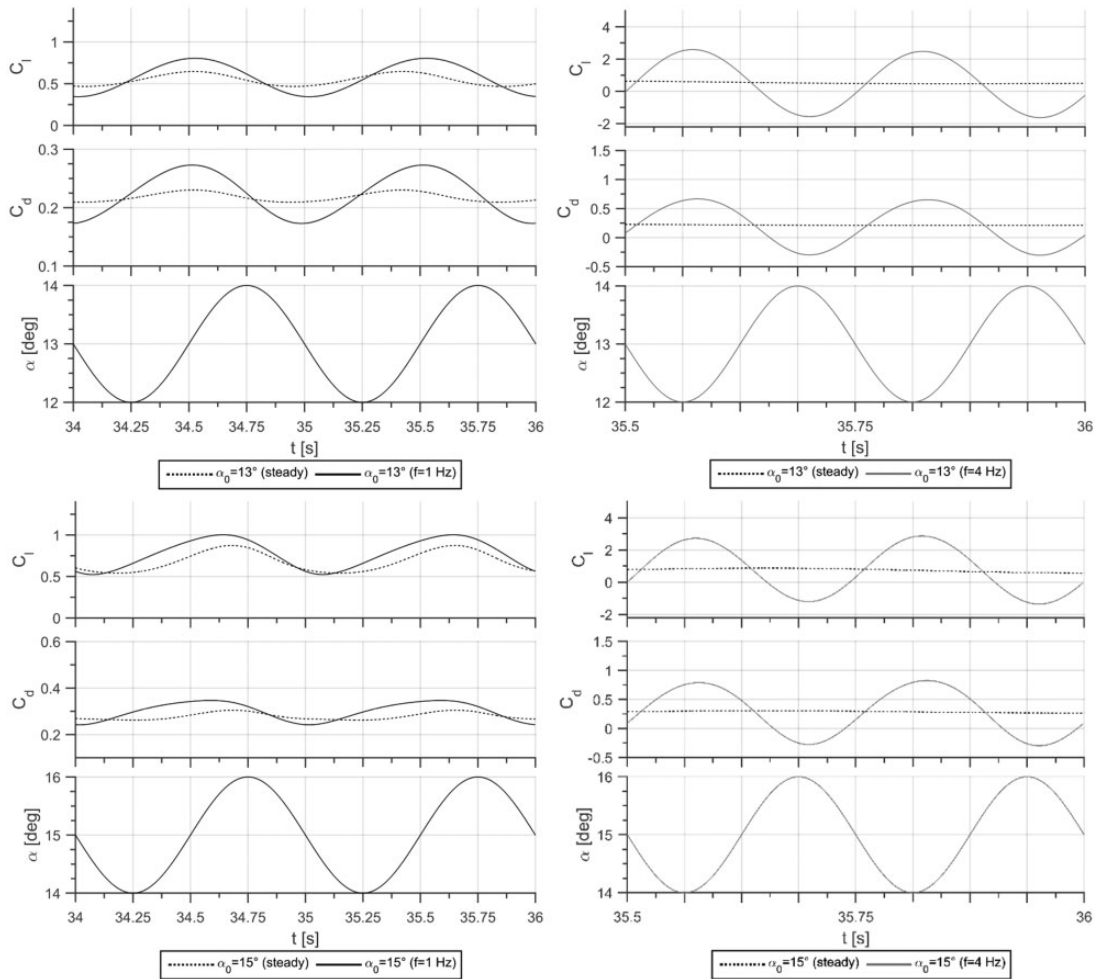


Figure 17. Instantaneous lift and drag coefficients for $f = 1$ Hz and $f = 4$ Hz oscillations at $\alpha_0 = 13^\circ$ and 15° .

Figure 18 shows the instantaneous lift and drag coefficients for higher mean angles of attack ($\alpha_0 = 40^\circ$ and 60°). At $f = 4$ Hz pitching oscillation, the sinusoidal behavior of the lift coefficient is observed throughout the period; however, it is not the case for $f = 1$ Hz oscillation. The amplitude of the lift and drag coefficients is very high for $f = 4$ Hz condition compared to $f = 1$ Hz oscillation and steady condition for these higher angles of attack. However, the amplitudes are comparable to each other for steady and $f = 1$ Hz oscillations. It is observed that C_l is almost equal to zero during a small interval for $f = 4$ Hz at $\alpha_0 = 40^\circ$, and C_d is slightly above the zero value at the same instances (Figure 18).

Amplitude spectrum, calculated using FFT algorithm, was determined based on the lift coefficient for the steady airfoil; this frequency peak (see Figure 19 and steady airfoil results in Figure 20) is due to vortex shedding from the airfoil. However, for

oscillating airfoils, in addition, the oscillation frequencies are observable in the amplitude spectrum.

At steady airfoil, the amplitude spectrum of lift coefficient does not show any peak until the angle of attack of 8° (Figure 19). At 8° angle of attack, a peak of very low amplitude is observed at a frequency of $f = 1.28$ Hz (Strouhal number of $St = fc/U_\infty = 0.876^{30}$). A maximum vortex shedding frequency of $f = 1.3$ Hz is observed at $\alpha_0 = 9^\circ$ (Figure 19) whose frequency amplitude can also be observed as dashed lines in Figure 20 at 9° angle of attack.

The frequency spectrum from 19° to 60° mean angles of attack reveals only a denser and higher amplitude low frequency spectrum as can be observed from Figures 20 and 21. It is known that for larger angles of attack, the frequency becomes smaller which implies that the shedding period of Karman vortices are longer. In literature, it is also denoted that as the shedding period increases with angle of attack, the

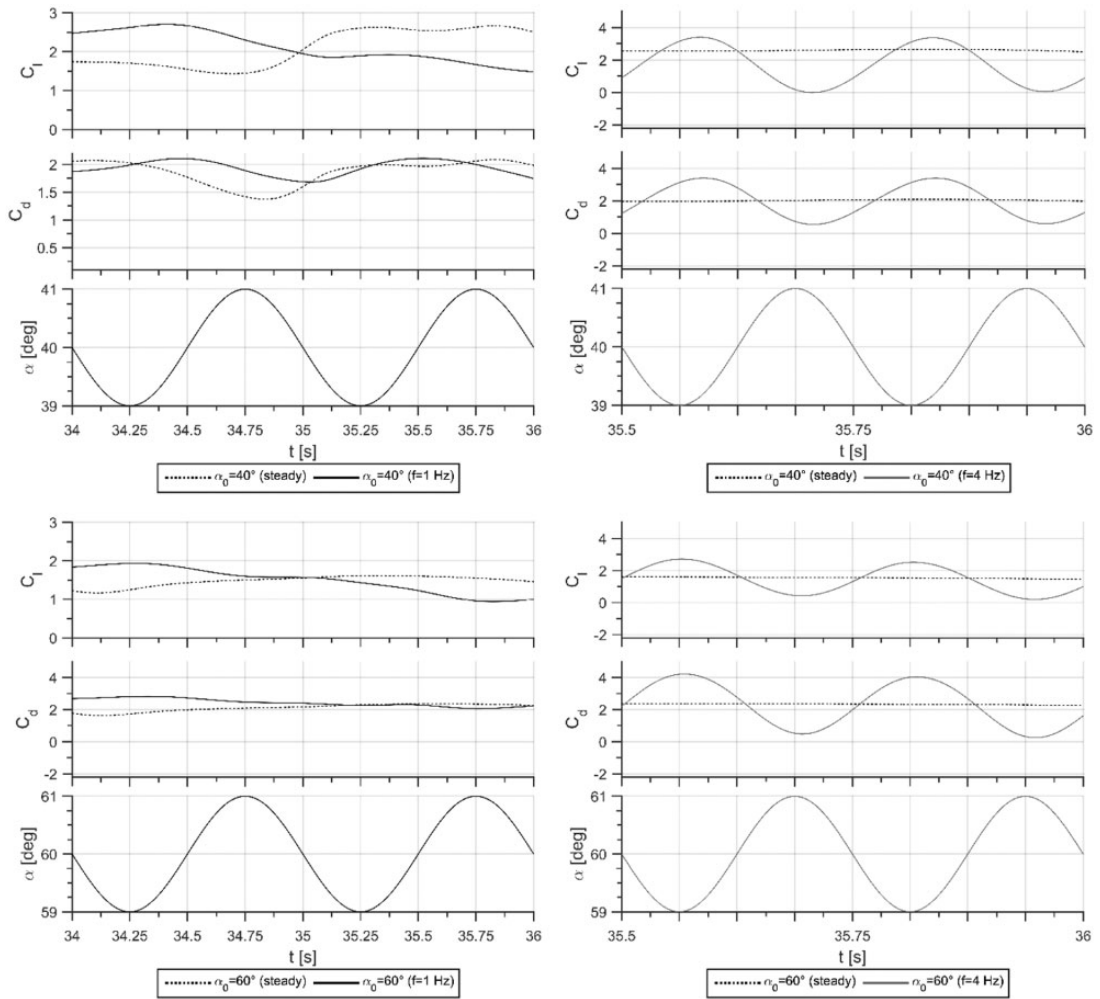


Figure 18. Instantaneous lift and drag coefficients for $f = 1$ Hz and $f = 4$ Hz oscillations at $\alpha_0 = 40^\circ$ and 60° .

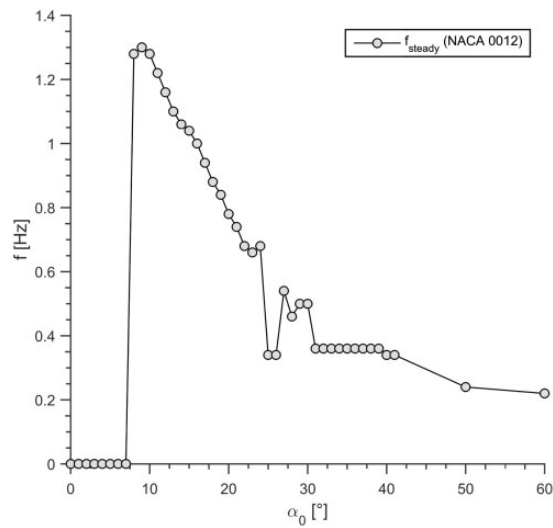


Figure 19. Shedding frequency for steady NACA 0012 airfoil at different angles of attack.

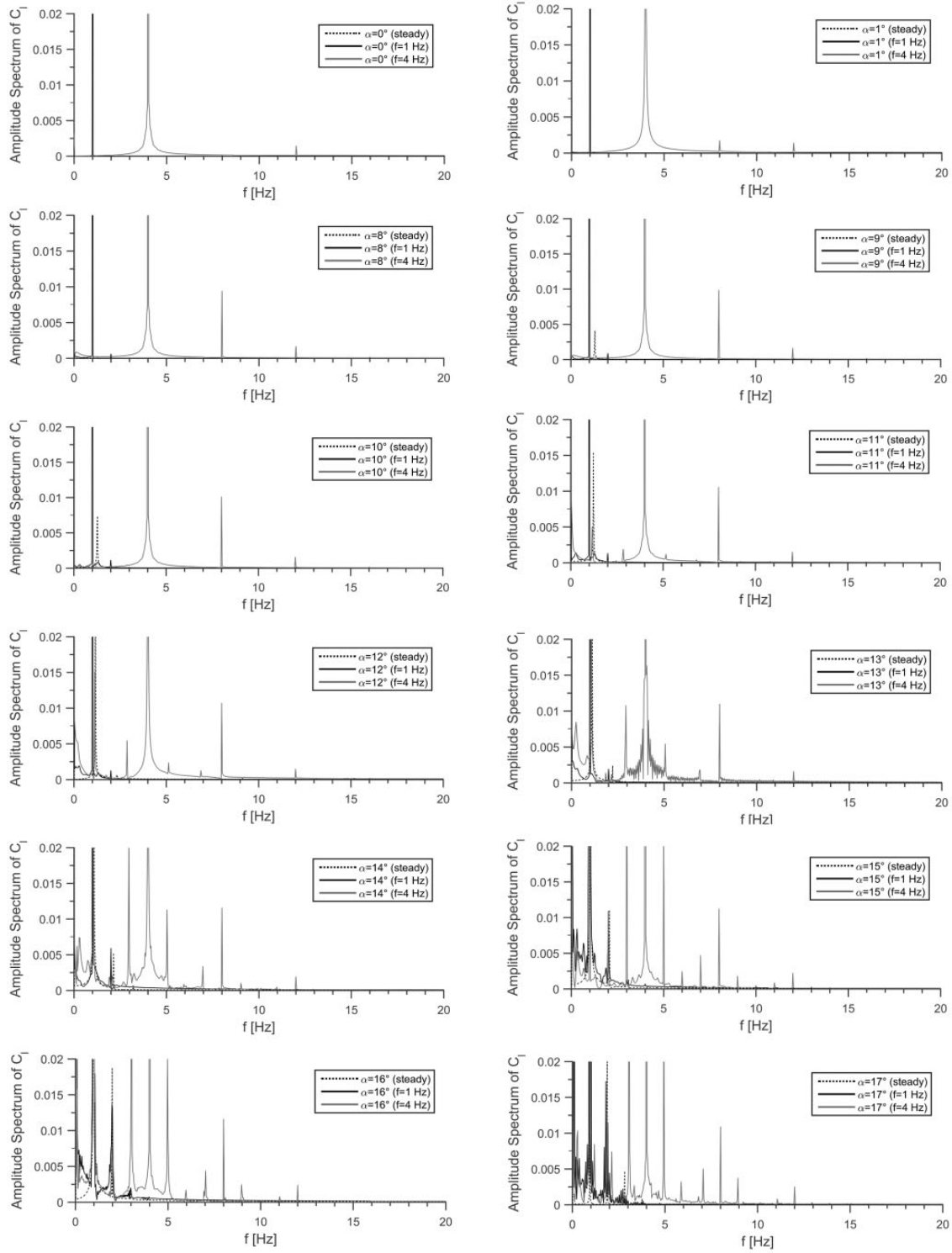


Figure 20. Amplitude spectrum of lift coefficients for $f = 1$ Hz and $f = 4$ Hz oscillations at $\alpha_0 = 0^\circ$ to 21° .

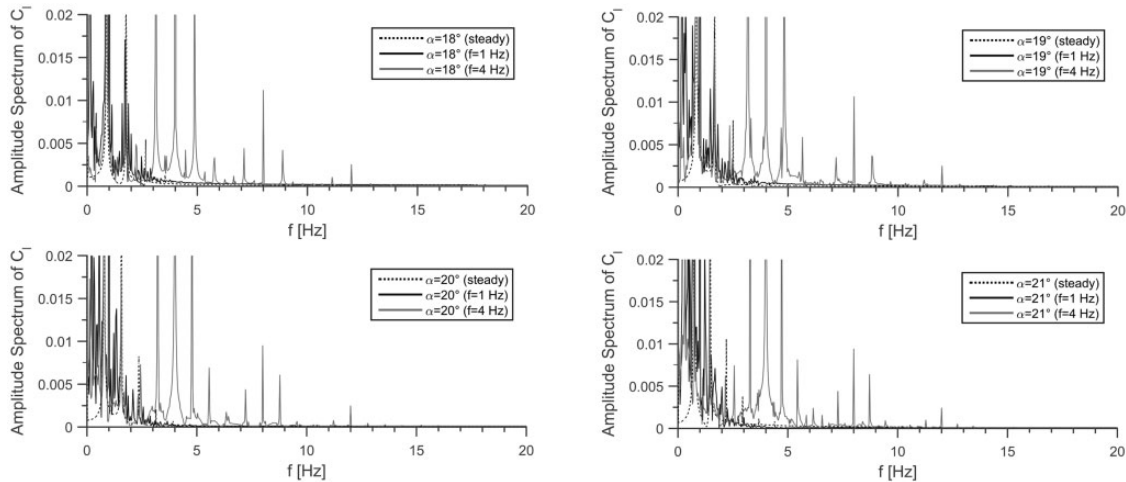


Figure 20. Continued.

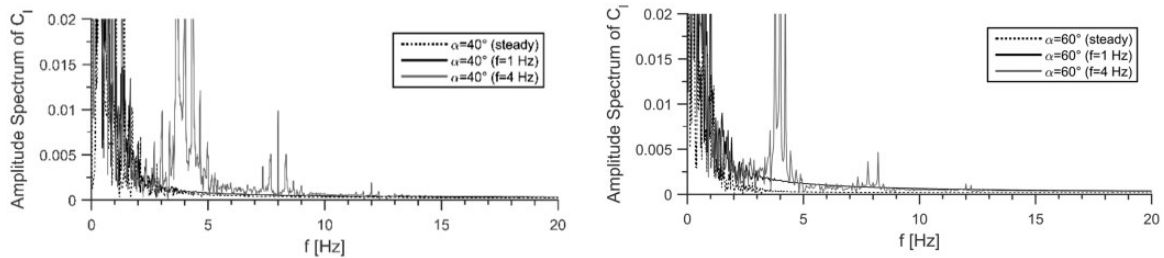


Figure 21. Amplitude spectrum of lift coefficients for $f = 1$ Hz and $f = 4$ Hz oscillations at $\alpha_0 = 40^\circ$ and 60° .

more K–H vortices are amalgamated to form one Karman vortex.^{30,40,41}

Conclusion

The numerical simulation of sinusoidally pitching NACA 0012 airfoil at $Re = 1000$ is performed at small amplitude oscillation of 1° . The computations are performed for mean angles of attack ranging from 0° to 60° and for pitching frequencies of 1 Hz and 4 Hz. Even at this small amplitude of oscillations, it is observed that the pitching frequency does not only alter the aerodynamic force coefficients but also the vortex shedding patterns of the airfoil. A periodic vortex shedding is observed above $\alpha_0 = 8^\circ$ for steady airfoil case and $\alpha_0 = 10^\circ$ for $f = 4$ Hz pitching airfoil which has created a delay effect on the unsteady wake formation at the downstream of the airfoil. In contrast, the periodic vortex shedding can be visualized for all angles of attack of the NACA 0012 airfoil oscillating at $f = 1$ Hz frequency.

A period doubling is observed in a sinusoidal form only for the drag coefficient at zero mean angle of attack at both oscillation frequencies. Negative instantaneous drag coefficients (thrust) are observed at $f = 4$ Hz pitching oscillation from mean angle of attack of 3° to 37° , but there is no thrust observation at $f = 1$ Hz oscillation for all angles of attack investigated.

Declaration of conflicting interests

The author(s) declared no potential conflicts of interest with respect to the research, authorship, and/or publication of this article.

Funding

The author(s) disclosed receipt of the following financial support for the research, authorship, and/or publication of this article: This work is supported by TUBITAK with project number 116M273.

ORCID iD

Dilek Funda Kurtulus  <https://orcid.org/0000-0002-0678-9474>

References

- Shyy W, Lian Y, Tang J, et al. *Aerodynamics of low Reynolds number flyers*. Cambridge Aerospace Series. Cambridge: Cambridge University Press, 2008.
- Shyy W, Aono H, Kang C-K, et al. *An introduction to flapping wing aerodynamics*, Cambridge Aerospace Series. Cambridge: Cambridge University Press, 2013.
- Mueller TJ. *Fixed and flapping wing aerodynamics for micro air vehicle applications*. USA: AIAA, 2001.
- Choudhuri PG, Knight DD and Visbal MR. Two-dimensional unsteady leading-edge separation on a pitching airfoil. *AIAA J* 1994; 32: 673–681.
- Wang S, Ingham DF, Ma L, et al. Turbulence modeling of deep dynamic stall at relatively low Reynolds number. *J Fluid Struct* 2012; 33: 191–209.
- Ko S and McCroskey WJ. Computations of unsteady separating flows over an oscillating airfoil. *AIAA J* 1997; 35: 1235–1238.
- Ashraf MA, Young J and Lai JCS. Reynolds number, thickness and camber effects on flapping airfoil propulsion. *J Fluid Struct* 2011; 27: 145–160.
- Yu M, Wang ZJ and Hu H. High fidelity numerical simulation of airfoil thickness and kinematics effects on flapping airfoil propulsion. *J Fluid Struct* 2013; 42: 166–186.
- Moriche M, Flores O and García-Villalba M. On the aerodynamic forces on heaving and pitching airfoils at low Reynolds number. *J Fluid Mech* 2017; 828: 395–423.
- Ardonceanu PL. Unsteady pressure distribution over a pitching airfoil. *AIAA J* 1989; 27: 660–662.
- Oshima H and Ramaprian BR. Velocity measurements over a pitching airfoil. *AIAA J* 1997; 35: 119–126.
- Métivier V, Dumas G and Poitrel D. Aeroelastic dynamics of a NACA 0012 airfoil at transitional Reynolds numbers. *AIAA J* 2009; 47: 1–18.
- Acharya M and Metwally MH. Unsteady pressure field and vorticity production over a pitching airfoil. *AIAA J* 1992; 30: 403–411.
- Lu K, Xie YH, Zhang D, et al. Numerical investigations into the asymmetric effects on the aerodynamic response of a pitching airfoil. *J Fluid Struct* 2013; 39: 76–86.
- McCroskey WJ. Inviscid flowfield of an unsteady airfoil. *AIAA J* 1973; 11: 1130–1137.
- Kim D-H and Chang J-W. Low-Reynolds-number effect on the aerodynamic characteristics of a pitching NACA 0012 airfoil. *Aerosp Sci Technol* 2014; 32: 162–168.
- Freymuth P. Propulsive vortical signature of plunging and pitching airfoils [Technical Notes]. *AIAA J* 1988; 26: 881–883.
- Koochesfahani MM. Vortical patterns in the wake of an oscillating airfoil. *AIAA J* 1989; 27: 1200–1205.
- Lai JCS and Platzer MF. The jet characteristics of a plunging airfoil. *AIAA J* 1999; 37: 1529–1537.
- Bohl DG and Koochesfahani MM. MTV measurement of the vertical field in the wake of an airfoil oscillating at high reduced frequency. *J Fluid Mech* 2009; 620: 63–88.
- Clever DJ, Wang Z, Gursul I, et al. Lift enhancement by means of small-amplitude airfoil oscillations at low Reynolds numbers. *AIAA J* 2011; 49: 2018–2033.
- Kurtulus DF, David L, Farcy A, et al. Aerodynamic characteristics of flapping motion in hover. *Exp Fluids* 2008; 44: 23–36.
- Tian W, Bodling A, Hong L, et al. An experimental study of the effects of pitch-pivot-point location on the propulsion performance of a pitching airfoil. *J Fluid Struct* 2016; 60: 130–142.
- Han C and Cho J. Unsteady aerodynamics analysis of flat plates in pitch oscillation. *AIAA J* 2006; 44: 1121–1126.
- Jones KD, Lund TC and Platzer MF. Experimental and computational investigation of flapping wing propulsion for micro air vehicles. In: Mueller TJ (ed.) *Fixed and flapping wing aerodynamics for micro air vehicles*. Chapter 16. USA: AIAA, 2001, pp.307–339.
- Sarkar S. Comparing pure-pitch and pure-plunge kinematics for a symmetric airfoil. *AIAA J* 2010; 48: 2962–2969.
- Sarkar S and Venkatraman K. Influence of pitching angle of incidence on the dynamic stall behavior of a symmetric airfoil. *Eur J Mech/B Fluids* 2008; 27: 219–238.
- Medjroubi W, Stoevesandt B, Carmo B, et al. High-order numerical simulations of the flow around a heaving airfoil. *Comput Fluids* 2011; 50: 68–84.
- Khalid MSU, Akhtar I and Durrani NI. Analysis of Strouhal number based equivalence of pitching and plunging airfoils and wake deflection. *Proc Inst Mech Eng G: J Aer Eng* 2015; 229: 1423–1434.
- Kurtulus DF. On the unsteady behavior of the flow around NACA 0012 airfoil with steady external conditions at $Re = 1000$. *Int J Micro Air Veh* 2015; 7: 301–326.
- Kurtulus DF. On the wake pattern of symmetric airfoils for different incidence angles at $Re = 1000$. *Int J Micro Air Veh* 2016; 8: 109–139.
- Rossi E, Colagrossi A, Oger G, et al. Multiple bifurcations of the flow over stalled airfoils when changing the Reynolds number. *J Fluid Mech* 2018; 846: 356–391.
- Kurtulus DF. Aerodynamic loads of small amplitude pitching NACA 0012 airfoil at Reynolds number of 1000. *AIAA J* 2018; 56: 3328–3331.
- Hoarau Y, Braza M, Ventikos Y, et al. Organized modes and the three dimensional transition to turbulence in the incompressible flow around a NACA0012 wing. *J Fluid Mech* 2003; 496: 63–72.
- Mittal S and Tezduyar TE. Massively parallel finite element computation of incompressible flows involving fluid-body interactions. *Comput Method Appl Mech Eng* 1994; 112: 253–282.
- Liu Y, Li K, Zhang J, et al. Numerical bifurcation analysis of static stall of airfoil and dynamic stall under unsteady perturbation. *Commun Nonlinear Sci Numer Simul* 2012; 17: 3427–3434.

37. Khalid MSU and Akhtar I. Characteristics of flow past a symmetric airfoil at low Reynolds number: a nonlinear perspective. In: *Proceedings of the ASME 2012 International Mechanical Engineering Congress and Exposition. Volume 7: Fluids and Heat Transfer, Parts A, B, C, and D*. Houston, Texas, USA. 9–15 November 2012, paper no. IMECE2012-87389, pp.167–175. ASME.
38. Suzuki T, Ji H and Yamamoto F. Unsteady PTV velocity field past an airfoil solved with DNS: part 1. Algorithm of hybrid simulation and hybrid velocity field at $Re = 10^3$. *Exp Fluids* 2009; 47: 957–976.
39. Kunz P and Kroo I. Analysis and design of airfoils for use at ultra-low Reynolds numbers. In: *Proceedings of AIAA fixed, flapping and rotary wing vehicles at very low Reynolds numbers conference*, Notre Dame, 5–7 June 2000, pp.349–372. University of Notre Dame, Notre Dame, IN: AIAA.
40. Mahbub Alam M, Zhou Y, Yang HX, et al. The ultra-low Reynolds number airfoil wake. *Exp Fluids* 2010; 48: 81–103.
41. Yarusevych S, Sullivan PE and Kawall JG. On vortex shedding from an airfoil in low-Reynolds number flows. *J Fluid Mech* 2009; 632: 245–271.